2-2022

Cu 2+ and Cu 3+ Acceptors in β-Ga 2 O 3 Crystals: A Magnetic Resonance and Optical Absorption Study

Timothy D. Gustafson

Nancy C. Giles
Air Force Institute of Technology

Brian C. Holloway

Christopher A. Lenyk
Air Force Institute of Technology

J. Jesenovec

See next page for additional authors

Recommended Citation

T. D. Gustafson, N. C. Giles, B. C. Holloway, C. A. Lenyk, J. Jesenovec, J. S. McCloy, M. D. McCluskey, and L. E. Halliburton , "Cu2+ and Cu3+ acceptors in β-Ga2O3 crystals: A magnetic resonance and optical absorption study", Journal of Applied Physics 131, 065702 (2022) https://doi.org/10.1063/5.0080502

Journal of Applied Physics

Cu^{2+} and Cu^{3+} acceptors in β-Ga_2O_3 crystals: A magnetic resonance and optical absorption study

T. D. Gustafson,[1,a)] N. C. Giles,[1] B. C. Holloway,[1] C. A. Lenyk,[1] J. Jesenovec,[2,3] J. S. McCloy,[2,3] M. D. McCluskey[2,4] and L. E. Halliburton,[5,a)]

[1]Department of Engineering Physics, Air Force Institute of Technology, Wright-Patterson Air Force Base, Ohio 45433, USA

[2]Institute of Materials Research, Washington State University, Pullman Washington, 99164 USA

[3]Materials Science and Engineering Program, Washington State University, Pullman, Washington, 99164, USA

[4]Department of Physics and Astronomy, Washington State University, Pullman, Washington, 99164, USA

[5]Department of Physics and Astronomy, West Virginia University, Morgantown, West Virginia 26506, USA

Abstract

Electron paramagnetic resonance (EPR) and optical absorption are used to characterize Cu^{2+} ($3d^9$) and Cu^{3+} ($3d^8$) ions in Cu-doped β-Ga_2O_3. These Cu ions are singly ionized acceptors and neutral acceptors, respectively (in semiconductor notation, they are Cu^- and Cu^0 acceptors). Two distinct Cu^{2+} EPR spectra are observed in the as-grown crystals. We refer to them as Cu^{2+}(A) and Cu^{2+}(B). Spin-Hamiltonian parameters (a *g* matrix and a ^{63,65}Cu hyperfine matrix) are obtained from the angular dependence of each spectrum. Additional electron-nuclear double resonance (ENDOR) experiments on Cu^{2+}(A) ions give refined ^{63}Cu and ^{65}Cu hyperfine matrices and provide information about the nuclear electric quadrupole interactions. Our EPR results show that the Cu^{2+}(A) ions occupy octahedral Ga sites with no nearby defect. The Cu^{2+}(B) ions, also at octahedral Ga sites, have an adjacent defect, possibly an OH^- ion, an oxygen vacancy, or an H^- ion trapped within an oxygen vacancy. Exposing the crystals at room temperature to 275 nm light produces Cu^{3+} ions and reduces the number of Cu^{2+}(A) and Cu^{2+}(B) ions. The Cu^{3+} ions have an S = 1 EPR spectrum and are responsible for broad optical absorption bands peaking near 365, 422, 486, 599, and 696 nm. Analysis of loops observed in the Cu^{3+} EPR angular dependence gives 2.086 for the g value

and 22.18, 3.31, and –25.49 GHz for the principal values of D (the fine-structure matrix). Thermal anneal studies above room temperature show that the Cu^{3+} ions decay and the Cu^{2+} ions recover between 75 and 375 °C.

[a)]Email addresses: Timothy.Gustafson@protonmail.com and Larry.Halliburton@mail.wvu.edu

I. INTRODUCTION

Copper serves as a deep acceptor in β-Ga_2O_3 and provides compensation for unintentional donors. Unlike the Zn acceptors in this wide bandgap semiconductor,[1-3] singly ionized and neutral Cu acceptors differ only in the number of *d* electrons. The neutral Zn acceptors are small polarons where the hole is localized on one oxygen neighbor and the 3d shell of the Zn ion remains filled.[1] In contrast, the neutral Cu acceptors in β-Ga_2O_3 have the hole localized in the 3d shell. The singly ionized acceptors are Cu^{2+} ions (with the $3d^9$ configuration) and the neutral acceptors are Cu^{3+} ions (with the $3d^8$ configuration). As a result, the Cu acceptors are deep in β-Ga_2O_3 and are not expected to produce p-type conductivity.[4] An interesting and unique property of the Cu acceptors in β-Ga_2O_3 (not seen with the more traditional Mg and Zn acceptors) is a significant photochromic response.[5] Exposure to 275 nm light converts Cu^{2+} ions to Cu^{3+} ions and produces broad optical absorption bands in the visible and near ultraviolet regions. [Note: Throughout this report, ionic notation is used for the Cu acceptors, with an emphasis on the d shell occupancy. In semiconductor notation, the singly ionized and neutral acceptors are Cu^- and Cu^0, respectively.]

In the present paper, we use electron paramagnetic resonance (EPR) and electron-nuclear double resonance (ENDOR) to characterize Cu^{2+} and Cu^{3+} ions in β-Ga_2O_3 crystals. These experimental techniques are well-suited to determine the electronic structure of the ground states of the Cu ions.[6,7] Two distinct S = 1/2 EPR spectra from Cu^{2+} ions at octahedral Ga sites are observed in the as-grown Cu-doped crystals. The responsible ions are referred to as Cu^{2+}(A) and Cu^{2+}(B). A third EPR signal, with S = 1, is produced at room temperature with 275 nm light and is assigned to Cu^{3+} ions at an octahedral Ga site. Spin-Hamiltonian parameters are extracted from the angular dependence of each spectrum and atomic-scale models are developed. The Cu^{2+}(A) and Cu^{3+} spectra are the expected singly ionized and neutral Cu acceptors, respectively, in β-Ga_2O_3. They

have no nearby defects. In contrast, the Cu^{2+}(B) ions have a defect at a nearest-neighbor oxygen site in the *b*-*c* plane. This perturbing defect is not identified in our study, but likely candidates are an OH^- ion, an oxygen vacancy, or an H^- ion trapped within an oxygen vacancy.

The present paper also describes the optical absorption features that are produced at room temperature with 275 nm light. Broad photoinduced absorption bands attributed to Cu^{3+} ions have peaks near 365, 422, 486, 599, and 696 nm. The 422, 599, and 696 nm bands are polarized (they are best seen with E ∥ *b*). After an exposure to 275 nm light, the three EPR spectra and the optical absorption bands are monitored during a series of thermal anneals at progressively higher temperatures (between 75 and 375 °C). These decay and recovery results help unravel the complexities of the roles played by the various defects in trapping electrons and holes during optical excitation of the Cu-doped β-Ga_2O_3 crystals.

There have been only a few studies of d^8 ions that are relevant to our present investigation. The observation of EPR spectra from Cu^{3+} and Ni^{2+} ions has been reported in α-Al_2O_3 crystals, a material similar to β-Ga_2O_3.[8,9] These papers provide insights as to the expected properties of the Cu^{3+} ions in β-Ga_2O_3 crystals. Although optically detected magnetic resonance (ODMR) has revealed the presence of Cu^{2+} ions,[10] there are no indications in the literature that stable Cu^{3+} ions can be formed in GaN. There are also no reports of EPR signals from Cu^{3+} ions in other III-V materials such as GaP and GaAs. The present paper provides a rare opportunity to establish the EPR and optical absorption properties of a d^8 ion in an important ultrawide-bandgap semiconductor.

II. EXPERIMENTAL DETAILS

The Cu-doped β-Ga_2O_3 crystals used in the present study were grown at Washington State University by the Czochralski (CZ) and vertical gradient freeze (VGF) methods.[2,5,11,12] An iridium crucible was employed and the Cu doping level in the starting materials was 0.25 at. %. Growth proceeded in two steps. The initial seeding and pulling portion of the growth occurred over approximately 12 h. A pulling rate of about 2 mm/h was used. The CZ growth was then removed and the remaining melt was slowly cooled at an approximate rate of 1-2 °C/min to produce the VGF boule. Reference 13 provides additional growth details. The Cu content in the VGF material

is an order of magnitude greater than in the CZ material.[13] An increased hydrogen content is expected to accompany the increased Cu content. In general, the CZ and VGF crystals will not necessarily be similar because of variations in stoichiometry, nonuniform distributions of defects, and leaching of impurities from the crucible.

Small rectangular-shaped samples, approximately 2 mm on a side, were cut from the larger boules. EPR verified that unintentional Ir^{4+} and Fe^{3+} ions are present in the as-grown crystals. The observation of Fe is important, as the known angular dependence[14] of the EPR spectrum from Fe^{3+} ions at octahedral Ga sites is used to precisely align the static external magnetic field along the crystal axes. In an earlier growth study, Galazka *et al*.[15] identified the evaporation of Cu due to a high partial pressure as a problem when growing Cu-doped β-Ga_2O_3 crystals by the Czochralski method. A small overpressure (20 kPa) inside the furnace during growth helped to suppress Cu evaporation in the current study.[13]

At various places in the present paper, EPR is used to obtain the concentrations of defects. This is done by comparing the area under the EPR absorption signal (i.e., after integrating the first-derivative signal) to the area under the signal from a standard Bruker weak-pitch sample containing a known number of spins. With this method, relative concentrations of defects in a crystal are determined more precisely than absolute concentrations. We estimate that our absolute concentrations are accurate to within a factor of two (a primary source of error is the uncertainty in knowing the number of spins in the standard sample). An advantage of using EPR to determine defect concentrations is its ability to focus on specific charge states. Comparison to the Bruker weak-pitch EPR standard gave a concentration of 5.1×10^{18} cm^{-3} for the Ir^{4+} ions in an as-grown CZ crystal. A separate infrared absorption measurement[16] of the intensity of the peak at 5153 cm^{-1} (1.94 μm) in the same sample gave 4.0×10^{18} cm^{-3} for the Ir^{4+} concentration, thus confirming the EPR result. The Fe^{3+} concentration, obtained from EPR, was approximately a factor of five lower than the Ir^{4+} concentration in this as-grown CZ sample. The Cu dopant and the unintentional impurities are not expected to be uniformly distributed in these boules.[13]

The β-Ga_2O_3 crystals have a monoclinic structure described by space group C2/m (C_{2h}^3),

with lattice constants a = 12.214 Å, b = 3.0371 Å, c = 5.7981 Å, and β = 103.83° at 273 K.[17,18] Following the usual convention, the b direction is perpendicular to the mirror plane. The angle between the a and c axes is β and the c^* direction is defined to be perpendicular to the a-b plane. There are equal numbers of tetrahedral and octahedral Ga sites in the crystal, labeled Ga(1) and Ga(2), respectively. Oxygen ions occupy three crystallographically inequivalent sites in the crystal, labeled O(I), O(II), and O(III), and are distinguished by the number and types of Ga neighbors.

A Bruker EMX spectrometer, with a cylindrical TM_{110} resonator, was used to acquire the EPR spectra. ENDOR spectra were taken with a Bruker Elexsys E-300 spectrometer and a cylindrical TE_{011} resonator. These X-band spectrometers operated near 9.38 GHz and 9.49 GHz, respectively. In the ENDOR experiments, the source of radio frequencies (restricted to the 1-120 MHz range) was frequency-modulated at 12.5 kHz. This gave first-derivative ENDOR signals. Oxford Instruments ESR-900 helium-gas flow systems were used to control the sample temperature and a Bruker NMR gaussmeter provided corrections for the small difference in the magnetic field at the sample and the spectrometer's Hall sensor located on a magnet pole cap. A 275 nm LED from Thorlabs (Model M275L4), with an output power of 45 mW, was used to convert Cu^{2+} ions to Cu^{3+} ions. The effects of 325 and 442 nm wavelengths from a Kimmon IK Series He-Cd laser were also investigated. Optical absorption spectra were taken with a Cary 5000 spectrophotometer and an ultrabroadband (250 nm to 4 μm) fused-silica wire-grid polarizer (Thorlabs Model WP25M-UB). The optical absorption spectra were not corrected for surface reflection losses and scattering.

III. EPR FROM Cu^{2+} IONS

Two distinct Cu^{2+} (S = 1/2) EPR spectra, with resolved hyperfine structure, are observed in the as-grown Cu-doped β-Ga_2O_3 crystals. One spectrum, labeled Cu^{2+}(A), is best seen at temperatures below 80 K. Although the responsible defect is present at room temperature, short spin-lattice relaxation times cause its lines to broaden beyond recognition at the higher temperatures. The second spectrum, labeled Cu^{2+}(B), can be easily seen at room temperature. The relative concentrations of the Cu^{2+}(A) and Cu^{2+}(B) ions depend on the growth conditions and vary from sample to sample. Results from two representative samples are included in our present study. Sample 1

was grown by the CZ method and has approximately equal initial concentrations of Cu^{2+}(A) and Cu^{2+}(B) ions. Sample 2 was grown by the VGF method and has an initial combined concentration of Cu^{2+}(A) and Cu^{2+}(B) ions that is slightly more than double that in Sample 1. More important, the distribution of Cu among the two defects is very different in Samples 1 and 2. When compared to Sample 1, the initial concentration of Cu^{2+}(A) ions is three times less in Sample 2 and the initial concentration of Cu^{2+}(B) ions is four times greater in Sample 2. More simply stated, in Sample 2 the concentration of Cu^{2+}(B) ions is about 12 times greater than the concentration of Cu^{2+}(A) ions. This is much different than the nearly equal concentrations found in Sample 1. A second distinguishing feature for the two samples is the Fermi level: it is higher in Sample 2 than in Sample 1. The EPR, ENDOR, and optical absorption results in Sections III, IV, V, and VI were obtained from Sample 1, while the thermal decay results in Section VII were obtained from Samples 1 and 2.

Most of the Cu^{2+} ions in our Cu-doped β-Ga_2O_3 crystals are located at octahedral Ga(2) sites. A few may also be at tetrahedral Ga(1) sites. Interstitial sites are unlikely for the Cu defects we observe. Thus far, computational studies of formation energies have found that Cu favors octahedral sites in β-Ga_2O_3.[4,5,19-21] For both the fourfold Ga(1) and the sixfold Ga(2) sites, the Cu^{2+} ion is slightly larger than the Ga^{3+} ion. The effective ionic radii of Ga^{3+} and Cu^{2+} ions at fourfold sites are 47 and 57 pm, respectively, and their effective radii at sixfold sites are 62 and 73 pm.[22] Closed shell Cu^{+} ions have effective ionic radii of 60 and 77 pm at the fourfold and sixfold sites.

A. Cu^{2+}(A) ions

Figure 1 shows EPR spectra from the Cu^{2+}(A) ions. These data were taken at 40 K from Sample 1 (a CZ-grown crystal). The microwave frequency was 9.379 GHz and the magnetic field was aligned along the *a*, *b* and *c** directions in Figs. 1(a), 1(b), and 1(c), respectively. Comparison to a Bruker weak-pitch EPR standard sample gave an approximate concentration of 8.4×10^{18} cm^{-3} for these Cu^{2+}(A) ions. A stick diagram above the spectrum in Fig. 1(a) identifies the four Cu hyperfine lines resulting from the I = 3/2 nuclear spins of the ^{63}Cu and ^{65}Cu isotopes. Selection rules ($\Delta M_S = \pm 1$ and $\Delta m_I = 0$) for the allowed EPR transitions give 2I+1 lines. The natural abundances of the ^{63}Cu and ^{65}Cu isotopes are 69.15% and 30.85%, respectively, and their magnetic

moments are $^{63}\mu = 2.2272\beta_n$ and $^{65}\mu = 2.3816\beta_n$, where β_n is the nuclear Bohr magneton.[23] Because the two isotopes have the same nuclear spin and similar magnetic moments, individual lines from the ^{63}Cu and ^{65}Cu nuclei are not resolved in Fig. 1 and only one set of four lines is observed for each direction of magnetic field. In Figs. 1(b) and 1(c), two smaller, and slightly broader, lines from Cu^{2+}(B) ions are present just to the high-field side of the four lines from the Cu^{2+}(A) ions.

Figure 2 shows the angular dependence of the Cu^{2+}(A) EPR spectrum. Data were taken at 40 K while rotating the direction of the magnetic field in 10° steps from *a* to *b*, *b* to *c**, and *c** to *a*. The following spin-Hamiltonian, containing an electron Zeeman term, a hyperfine term, and a nuclear Zeeman term, describes these results.

$$H = \beta \mathbf{S}\cdot\mathbf{g}\cdot\mathbf{B} + \mathbf{I}\cdot\mathbf{A}\cdot\mathbf{S} - g_n\beta_n\mathbf{I}\cdot\mathbf{B}. \quad (1)$$

The g and A matrices in Eq. (1) each have six independent parameters. These are the three principal values and the three Euler angles that define the directions of the principal axes. In Fig. 2, the EPR lines do not split into two branches in the middle portions of the *a*-*b* and *b*-*c** planes (although splittings in these planes are often seen for defects in monoclinic crystals).[24,25] The lack of splitting indicates that the principal axes of the g and A matrices for the Cu^{2+}(A) ions are near the *a*, *b*, and *c** directions in the crystal. To extract values for the 12 parameters, the spin Hamiltonian in Eq. (1) was rewritten as an 8 × 8 matrix (S = 1/2, I = 3/2) using the $|M_S, m_I\rangle$ basis set. This matrix was then repeatedly diagonalized (to obtain the energy eigenvalues) in a least-squares fitting routine. Input data for the fitting were the 177 pairs of magnetic field values and microwave frequencies representing the experimental points in Fig. 2. In the fitting process, the parameters in the g and A matrices were systematically varied until the predicted line positions agreed with the measured positions. "Best-fit" values for the spin-Hamiltonian parameters are listed in Table I. The Euler angles for each matrix have been converted in Table I to polar and azimuthal (θ,ϕ) pairs of angles, where θ is relative to the *c** axis and ϕ is relative to the *a* axis with positive rotation being from *a* toward *b* in the plane perpendicular to *c**. Principal values of the hyperfine matrix in Table I represent a "weighted average" of the two isotopes since individual lines from the ^{63}Cu and ^{65}Cu nuclei are not resolved in the EPR spectra. Recently, an EPR spectrum with similar spin-Hamil-

tonian parameters was assigned to Cu^{2+} ions unintentionally present in β-Ga_2O_3 powder.[26]

The results in Table I allow us to develop a model for the Cu^{2+}(A) ions in β-Ga_2O_3. First, we review the notation and the coordinate system used to describe d orbitals. A "free" Cu^{2+} ($3d^9$) ion has a $^2D_{5/2}$ ground state (S = 1/2, L = 2). Within the crystal, in the presence of the crystalline electric field, the degeneracy of the five d orbitals is partially removed and only the lowest-lying states are thermally populated.[27] For a Cu^{2+} ion at the slightly distorted octahedral Ga(2) site in β-Ga_2O_3, the lowest state (occupied by the unpaired spin) will be either ($3z^2 - r^2$) or ($x^2 - y^2$). The (xy), (yz), and (xz) states are much higher in energy. If the Cu^{2+} ions were instead at a tetrahedral site, the ordering of the T_{2g} and E_g states would be reversed. The x, y, and z directions used to describe d orbitals at the octahedral Ga(2) site are defined within the GaO_6 octahedron, and thus do not correspond to the *a*, *b*, *c* crystal axes in the β-Ga_2O_3 crystal. We take the z direction to be near the *a* axis in the crystal, the x direction to be between the *b* and –*c* directions, and the y direction to be between the *b* and *c* directions). This places the six neighboring oxygen ions in pairs around the Ga(2) site, roughly along the x, y, and z directions.

The g matrix for the Cu^{2+}(A) ions (see Table I) is approximately axial with $g_{\parallel} < g_{\perp}$. Its unique principal axis, associated with the smallest g value, is near the *a* direction in the crystal (or equivalently, the z direction). The two remaining perpendicular principal axes, corresponding to the larger, slightly inequivalent, g values, are close to the *b* and *c* directions in the crystal. An orthorhombic distortion is responsible for the minor inequivalence in these latter two g values and places their principal-axis directions nearly midway between the x and y and the x and –y directions. The ordering of the principal g values (one smaller and two larger) is consistent with a model that has the Cu^{2+} ion at an octahedral Ga(2) site. An analysis of g matrices for $3d^9$ ions,[28-30] when combined with our experimental g matrix in Table I, places the Cu^{2+}(A) unpaired spin (i.e., the hole) in a ($3z^2 - r^2$) orbital aligned near the crystal's *a* axis. A small contraction of the octahedron along the z direction or, equivalently, an expansion along x and y favors the ($3z^2 - r^2$) orbital for the unpaired spin rather than the ($x^2 - y^2$) orbital. There is no evidence from EPR that Cu^{2+}(A) ions have a nearby perturbing defect.

B. Cu^{2+}(B) ions

EPR spectra from the Cu^{2+}(B) ions in β-Ga_2O_3 are shown in Fig. 3. The data in Figs. 1 and 3 were obtained from Sample 1, but with different measurement temperatures (40 K in Fig. 1 and room temperature in Fig. 3). At room temperature, the lines in the Cu^{2+}(A) spectrum are too broad to observe. The magnetic field was aligned along the *a*, *b* and *c** directions in Figs. 3(a), 3(b), and 3(c), respectively. In Fig. 3, the approximate concentration of Cu^{2+}(B) ions is 9.7×10^{18} cm^{-3}. The four Cu hyperfine lines are identified by a stick diagram above the spectrum in Fig. 3(b). When the magnetic field is along the *a* direction, the separation between the four lines is reduced to near zero and only a broad slightly distorted line is seen. Additional lines in Fig. 3, marked with asterisks, are from Fe^{3+} ions at octahedral Ga(2) sites.

The angular dependence of the Cu^{2+}(B) EPR spectrum, taken at room temperature, is shown in Fig. 4. These data were obtained while rotating the direction of the magnetic field from *a* to *b*, *b* to *c**, and *c** to *a*. The splitting of the EPR spectrum into two branches in the *b*-*c** plane in Fig. 4 indicates that there are two crystallographically equivalent, but magnetically inequivalent, orientations of the Cu^{2+}(B) ions.[25] The fitting method described in Section III A, combined with the spin-Hamiltonian in Eq. (1), was used to extract g and A matrices from the angular dependence of the Cu^{2+}(B) EPR spectrum. Input data were the 169 pairs of magnetic field values and microwave frequencies representing the experimental points in Fig. 4. The resulting "best-fit" values for the Cu^{2+}(B) parameters are listed in Table II. Directions of the principal axes in Table II are for one of the two crystallographically equivalent orientations of the Cu^{2+}(B) ions. The principal-axis directions for the other orientation are obtained by applying a reflection through the mirror plane of the crystal to the matrices in Table II. Principal values of the hyperfine matrix in Table II are again a "weighted average" for the ^{63}Cu and ^{65}Cu isotopes.

As can be seen when comparing the results in Tables I and II, the g matrices and the hyperfine matrices are significantly different for the Cu^{2+}(A) and Cu^{2+}(B) ions. Fitting the EPR angular dependence gave $g_{\parallel} < g_{\perp}$ for the Cu^{2+}(A) ions. A similar process gave $g_{\parallel} > g_{\perp}$ for the Cu^{2+}(B) ions. The g matrices for both defects are axial, but the direction of the unique principal

axis is near the *a* direction for the Cu^{2+}(A) ions and between the *b* and *c** directions for one of the crystallographically equivalent orientation of the Cu^{2+}(B) ions (and between the $-b$ and *c** directions for the other orientation). In Table II, the hyperfine matrix for the Cu^{2+}(B) ions is also axial with its unique axis between the *b* and *c** directions (the same as the unique axis of the g matrix).

Although the Cu^{2+}(A) and Cu^{2+}(B) EPR spectra both represent Cu^{2+} ions at an octahedral site, their different g and hyperfine matrices indicate that they do not have the same environment. When combined with the results in Section VII, we conclude that a defect is located near the Cu^{2+}(B) ion. A different x, y, z coordinate system, then, is needed when describing the d orbitals. For the orientation of the Cu^{2+}(B) ion described in Table II, the z direction is placed midway between *b* and *c* (i.e., along the unique axes of the g and hyperfine matrices), the x direction is near *a*, and the y direction is midway between *b* and $-c$. With these x, y, and z directions, the g matrix in Table II is consistent with the unpaired spin (i.e., the hole) occupying an $(x^2 - y^2)$ orbital.[28-30] A defect with an effective positive charge located at the oxygen site along the z direction makes the hole prefer the $(x^2 - y^2)$ orbital rather than the $(3z^2 - r^2)$ orbital.

Candidates for this adjacent defect are an OH^- ion, an oxygen vacancy, or an H^- ion trapped within an oxygen vacancy. The observation of the two crystallographically equivalent, but magnetically inequivalent, orientations of the Cu^{2+}(B) ions (demonstrated by the splitting of the EPR spectrum into two branches in the *b*-*c** plane in Fig. 4) indicates that the perturbing defect is in the *b*-*c* plane at one of the four oxygen sites that are adjacent to the Ga(2) site where the Cu^{2+}(B) ion is located. More specifically, the perturbing defect is at one of the two O(I) sites or at one of the two O(III) sites. The defect could be on either site within a pair and thus would give two crystallographically equivalent orientations for the Cu^{2+}(B) ions. Our candidate defects (i.e., donors) have positive charge relative to the regular lattice and form a close-associate pair when next to a Cu^{2+} acceptor in the as-grown crystal. As an example of a nearby perturbation,[31] we note that a Cu^{2+} ion substituting for a Ti^{4+} ion in TiO_2, with an adjacent oxygen vacancy, has g and hyperfine matrices that are similar to those reported in Table II for the Cu^{2+}(B) ions.

IV. ENDOR FROM Cu^{2+}(A) IONS

Electron-nuclear double resonance (ENDOR) experiments are often used to identify nuclei that participate in an EPR spectrum. In our present case, it is already known that ^{63}Cu and ^{65}Cu are responsible for the four-line EPR spectra in Figs. 1 and 3. ENDOR, however, does give other useful information, namely improved values of the Cu hyperfine parameters and, most important, the nuclear electric quadrupole matrix for the Cu nuclei. The strength of a quadrupole interaction is directly proportional to the electric field gradient at the nucleus. Because of the monoclinic crystal structure of β-Ga_2O_3, there is a large electric field gradient at each Cu^{2+} nucleus caused by the surrounding lattice (with enhancement by the Sternheimer antishielding factor).[32] The unpaired spin residing primarily in a d orbital also makes a significant contribution to the electric field gradient at the Cu^{2+} nucleus. EPR experiments, by themselves, do not usually provide information about the nuclear electric quadrupole interactions (except when forbidden transitions are observed).[31] With ENDOR, these interactions are directly measured.

Two representative ENDOR spectra obtained from the ^{63}Cu and ^{65}Cu nuclei in the Cu^{2+}(A) ions are shown in Fig. 5. The temperature is 13 K and the magnetic field is aligned along the *a* direction in the crystal. In an ENDOR experiment, the magnetic field is held constant at the center of an EPR line and the radio frequency (rf) is swept through a region of interest, giving signals when the rf has the appropriate energy to "flip" a nuclear spin (selection rules for the ENDOR transitions are $\Delta M_S = 0$ and $\Delta m_I = \pm 1$).[33] The ENDOR spectrum in Fig. 5(a) was taken with the magnetic field fixed at the second (i.e., next-to lowest) EPR line in Fig. 1(a) and the spectrum in Fig. 5(b) was taken with the magnetic field set at the third EPR line. Additional ENDOR lines, expected in the 150 to 165 MHz region, are not present in the spectra in Fig. 5. This is because the upper limit of the rf amplifier in our ENDOR spectrometer was nominally 100 MHz and only a few of the lines appearing at higher frequencies were detected. The label above each line in Fig. 5 identifies the responsible nucleus as ^{63}Cu or ^{65}Cu.

Figure 6 shows the complete ENDOR angular dependence for the ^{63}Cu nuclei in the Cu^{2+}(A) ions. The discrete points are experimental results. These data were taken while rotating the direc-

tion of the magnetic field from *a* to *b*, *b* to *c**, and *c** to *a*. The following spin-Hamiltonian was used to determine the parameters that describe the angular data in Fig. 6.

$$H = \beta \mathbf{S}\cdot\mathbf{g}\cdot\mathbf{B} + \mathbf{I}\cdot\mathbf{A}\cdot\mathbf{S} + \mathbf{I}\cdot\mathbf{P}\cdot\mathbf{I} - g_n\beta_n\mathbf{I}\cdot\mathbf{B}. \quad (2)$$

This is the same as the Hamiltonian in Eq. (1), except that a nuclear electric quadrupole term has been added. The nuclear electric quadrupole matrix P is traceless. Its principal values are proportional to e^2qQ, where eq is the electric field gradient and Q is the nuclear quadrupole moment. When using the fitting process to extract the A and P matrices from the angular dependence in Fig. 6, the g matrix was fixed at the values given in Table I. Input data were the 295 pairs of ENDOR frequencies and magnetic field values representing the experimental points in Fig. 6. The resulting "best-fit" values for the ^{63}Cu parameters are listed in Table III for the Cu^{2+}(A) ions. Corresponding values for the ^{65}Cu parameters are obtained by multiplying the hyperfine principal values in Table III by 1.069 and multiplying the quadrupole principal values by 0.924. These numerical factors are the ratios of nuclear magnetic moments and nuclear electric quadrupole moments, respectively, for the two Cu isotopes.[23] The principal-axis directions are the same for the two isotopes. For comparison, we note that Jeom and Lim[34] have used nuclear magnetic resonance (NMR) to determine the nuclear electric quadrupole parameters for ^{69}Ga and ^{71}Ga nuclei in β-Ga_2O_3 crystals.

V. EPR FROM Cu^{3+} IONS

An S = 1 EPR spectrum appears when the Cu-doped β-Ga_2O_3 crystals are exposed at room temperature to ultraviolet light. At the same time, the EPR spectra from the Cu^{2+}(A) and Cu^{2+}(B) ions decrease in intensity. For both Sample 1 and Sample 2, the underlying electronic process leading to formation of the S = 1 spectrum is efficiently driven by 275 nm (4.51 eV) light. We found that 325 nm (3.81 eV) light is considerably less efficient in both samples and 442 nm (2.81 eV) light has essentially no effect. This suggests that a threshold mechanism may be involved, with photon energies greater than mid-gap required.

The new S = 1 spectrum is assigned to Cu^{3+} ($3d^8$) ions. Although S = 1 spectra are usually studied with higher microwave frequencies,[35] we could easily identify lines due to the Cu^{3+} ions

using our spectrometer operating near 9.4 GHz. Figure 7 shows the Cu^{3+} EPR spectrum taken at room temperature from Sample 1 after an exposure to 275 nm light (the microwave frequency was 9.377 GHz and the magnetic field was along the *a* direction). The same Cu^{3+} spectrum, with nearly the same intensity, is produced with 275 nm light in Sample 2. Long spin-lattice relaxation times allow the Cu^{3+} ions to be observed at room temperature. We estimate that the concentration of Cu^{3+} ions in Fig. 7 is approximately 1.4×10^{19} cm^{-3}.

The following spin-Hamiltonian (with S = 1 and I = 3/2) describes the Cu^{3+} EPR spectrum:

$$H = \beta \mathbf{S} \cdot \mathbf{g} \cdot \mathbf{B} + \mathbf{S} \cdot \mathbf{D} \cdot \mathbf{S} + \mathbf{I} \cdot \mathbf{A} \cdot \mathbf{S} - g_n \beta_n \mathbf{I} \cdot \mathbf{B}. \quad (3)$$

Electron Zeeman, fine structure (i.e., zero-field splitting), hyperfine, and nuclear Zeeman terms are included.[36] Here, the D matrix represents the spin-orbit and spin-spin couplings between the 3d electrons averaged over their spatial distributions.[37] There are two groups of four lines, centered near 0.653 and 1.375 T, in the spectrum in Fig. 7. The separation of lines within each group is approximately 6.2 mT and is the result of hyperfine interactions with ^{63}Cu and ^{65}Cu nuclei. As expected, the strengths of these Cu^{3+} hyperfine interactions in β-Ga_2O_3 are similar to those reported for Cu^{3+} in α-Al_2O_3.[8] More important, the two sets of lines in Fig. 7 are separated by 0.722 T. This large separation is caused by the zero-field splitting and thus directly demonstrates the S = 1 nature of the Cu^{3+} spectrum.

The angular dependence of the Cu^{3+} EPR spectrum (for our X-band microwave frequency) is shown in Fig. 8. Data were taken for rotations in the *a*-*b* and the *b*-*c** planes. Here, we ignore the relatively small Cu hyperfine splittings and plot only the centers of the two four-line groups. This angular dependence is unusual, as lines are only detected when the direction of the magnetic field is near *a* or *c**. There were no EPR lines for most directions of magnetic field because the zero-field splittings are larger than our microwave frequency. The spin-Hamiltonian in Eq. (3), after removing terms involving the nuclear spin, is used to extract parameters from the experimental data in Fig. 8. We assume an isotropic g matrix, as our limited angular data does not allow a full determination of the g matrix. This is, however, a good approximation, since the anisotropy of g matrices is usually minimal for d^8 spin systems.[8,9] Because the loops in Fig. 8 are centered

on the *a* and the *c** directions, the principal axes of the D matrix must be along the *a*, *b*, and *c** directions in the crystal. Also, the D matrix is traceless. Together, this leaves only three parameters to be determined (a g value and two principal values of the D matrix). Input data for the fitting program were the microwave frequency (9.377 GHz), two magnetic fields from the *a* spectrum (0.653 and 1.375 T), and one magnetic field from the *c** spectrum (0.934 T). The "best-fit" values for the Cu^{3+} spin-Hamiltonian parameters are given in Table IV.

Figure 9 illustrates the origin of the "loops" in the Cu^{3+} angular dependence (see Fig. 8).[38,39] In this figure, energy levels are plotted versus the strength of the magnetic field (hyperfine effects are not included). The magnetic field is oriented along the *a* direction in Fig. 9(a) and is rotated 12° from *a* toward *b* in Fig. 9(b). EPR transitions are indicated by vertical red lines having lengths corresponding to the microwave frequency. With the field along *a*, the two EPR lines are separated by 722 mT, as seen in Fig. 9(a). When the direction of the magnetic field is rotated away from *a*, the two energy levels begin to separate and the two EPR lines move closer. At 12° in Fig. 9(b), they have moved to a separation of 518 mT. The two energy levels continue to diverge as the angle from *a* is increased and the EPR lines continue to converge. Beyond 18°, the separation between the two energy levels is greater than the microwave frequency and EPR transitions no longer occur.

VI. PHOTOINDUCED OPTICAL ABSORPTION

Figure 10 shows optical absorption from Sample 1 before and after an exposure to 275 nm light. These spectra were taken at room temperature with unpolarized light propagating along the *a* direction in the crystal. Two absorption peaks, near 2.90 eV (428 nm) and 3.48 eV (356 nm) are present in the "before light" spectrum. These absorption features have been attributed to the presence of deep singly ionized Ir^{4+} donors.[2,40] The primary effect of the 275 nm light is the production of a broad double-peaked absorption in the region from 2.4 to 3.7 eV (517 to 335 nm). These photoinduced absorption features have been assigned by Jesenovec *et al.*[5] to Cu^{3+} ions. Additional photoinduced absorption is seen between 1.6 and 2.3 eV (775 to 540 nm).

A more detailed look at the photoinduced absorption from Sample 1 is provided in Fig. 11. The spectra in this figure were taken at room temperature with light propagating along the *a* direc-

tion and polarized either E ∥ *b* or E ∥ *c**. Before the exposure to 275 nm light, only the absorption at the band edge shows a polarization effect, shifting from 4.70 eV for E ∥ *b* to 4.45 eV for E ∥ *c**. Intrinsic transitions from multiple valence bands to the conduction band minimum are responsible for this shift (selection rules govern their polarizations).[41-43] After the exposure to 275 nm light, significant polarization effects are seen in the photoinduced bands associated with the Cu^{3+} ions. Two bands peaking near 3.40 and 2.55 eV dominate the spectrum with E ∥ *c**. Additional absorption is seen with E ∥ *b*. In the inset to Fig. 11, the spectrum taken with E ∥ *c** has been subtracted from the spectrum taken with E ∥ *b*. The resulting "difference" spectrum shows an intense peak near 2.94 eV and smaller peaks near 2.07 and 1.78 eV. Our results in Fig. 11 suggest that there are five bands associated with the Cu^{3+} ions, two at 365 and 486 nm best seen with E ∥ *c** and three at 422, 599, and 696 nm best seen with E ∥ *b*. These same five absorption bands are also present, with similar intensities, in Sample 2 after exposure to 275 nm light.

Blumberg *et al*.[8] showed that the three absorption bands observed in the visible and near-ultraviolet for Cu^{3+} ions in α-Al_2O_3 are explained by a Tanabe-Sugano energy level diagram[44-46] constructed for $3d^8$ ions in a cubic field. A similar approach is appropriate for our present case. The Cu^{3+} ions in β-Ga_2O_3 are in a distorted octahedron and this should cause a further splitting of levels and possibly introduce polarization effects, thus supporting our assignment of the five photo-induced bands in Fig. 11 to Cu^{3+} ions. A theoretical/computational study of the expected optical absorption from Cu^{3+} ions in β-Ga_2O_3 will help in the interpretation of the experimental spectra.

Samples 1 and 2 differ in one respect. The two absorption bands attributed to Ir^{4+} ions, at 2.90 eV and 3.48 eV in the "before light" spectrum in Sample 1 (see Fig. 10), are not observed in the "before light" spectrum from Sample 2. This result indicates that the Fermi level is higher in Sample 2, with most of the iridium present as Ir^{3+} ions (i.e., neutral donors).

VII. THERMAL RECOVERY RESULTS

The decay of the Cu^{3+} EPR spectrum and Cu^{3+} optical absorption bands and the recovery of the Cu^{2+} EPR spectra have been monitored as a crystal is heated stepwise above room temperature. These results for Samples 1 and 2 are shown in Figs. 12, 13, 14, and 15. Before beginning

each series of thermal annealing steps, the crystal was reset by heating to 500 °C. This removed the effects of previous illuminations and restored the crystal to its as-grown state. Then, the crystal was exposed at room temperature to 275 nm light for 2 min. Next, the crystal was heated in 25 °C steps, from 75 to 375 °C. For each step, after pre-heating a small tube furnace to a set temperature, the crystal was quickly positioned at the center of the furnace and removed after 2 min. Following the 2 min anneal, the crystal was either placed in the microwave cavity and an EPR spectrum was taken at 40 K or placed in the spectrophotometer and an optical absorption spectrum was taken at room temperature. After recording the spectrum, the process was repeated at the next higher temperature. For each sample, EPR data were collected during one series of heating steps and optical absorption data were collected during an identical, but separate, series of heating steps.

Data describing the thermal decay of the Cu^{3+} optical absorption bands in Sample 1 (CZ-grown) are shown in Fig. 12. These spectra were taken with light propagating along the *a* direction in the crystal and polarized with $E \parallel b$. With this polarization of the spectrometer light, the bands peaking at 365, 422, and 486 nm are all present and strongly overlap. Although spectra were taken every 25 °C, only a subset of these spectra are plotted in Fig. 12. A similar set of absorption data for Sample 2 (VGF-grown) is shown in Fig. 13. The absorption bands in Figs. 12 and 13 are very similar, both in shape and intensity, which agrees with our observations in Section V that the concentrations represented by the Cu^{3+} EPR signal are nearly the same in Sample 1 and Sample 2. This leads us to conclude that the photoinduced optical absorption bands in Figs. 11 and 12 and the EPR spectrum in Fig. 7 are from the same defect, namely, the isolated Cu^{3+} neutral acceptor at an octahedral Ga site.

The thermal decay results for the EPR spectra observed in Sample 1 are shown in Fig. 14. Intensities of the Cu^{2+}(A), Cu^{2+}(B), Cu^{3+}, and Ir^{4+} EPR spectra are plotted as a function of heating temperature. Starting on the left side of the plot, the first two sets of data points represent intensities of the EPR spectra before and immediately after the exposure to the 275 nm light. The intensities of the Cu^{2+}(A), Cu^{2+}(B), and Ir^{4+} spectra are normalized to their initial values before 275 nm light and the intensity of the Cu^{3+} spectrum is normalized to its value immediately after illuminat-

ing with the 275 nm light. Heating steps begin with the data points at 75 °C. Normalized production and decay results for the optical absorption (measured at 422 nm in Fig. 12) are also included in Fig. 14. The Ir^{4+} and Cu^{2+}(A) EPR spectra both decrease by more than half and the Cu^{3+} EPR and optical absorption spectra appear when the 275 nm light is turned on, whereas heating in the 275-375 °C region restores the initial Ir^{4+} and Cu^{2+}(A) spectra and destroys the Cu^{3+} spectra. Although 275 nm light initially reduces both of their intensities, the Cu^{2+}(A) and Cu^{2+}(B) ions have significantly different recovery behaviors during the subsequent heating. There is a small decrease in the Cu^{3+} EPR spectrum in the 75 to 200 °C region that appears to correlate with the recovery of the Cu^{2+}(B) ions.

A relatively simple explanation of the primary photoinduced process emerges from the data in Fig. 14. In Sample 1, with a lower Fermi level, electrons and holes produced by the 275 nm light are trapped at Ir^{4+} ions and Cu^{2+}(A) ions, respectively, and form Ir^{3+} ions (neutral donors) and Cu^{3+} ions (neutral acceptors). In other words, the light transfers electrons from the singly ionized Cu^{2+}(A) acceptors to the singly ionized Ir^{4+} donors (e.g., an electron from the valence band is excited to an Ir^{4+} ion and the hole left in the valence band is trapped by a Cu^{2+} ion). Upon heating, the Ir^{3+} and Cu^{3+} ions become thermally unstable between 275 and 375 °C. One (or both) of these neutral defects release charge that then moves to the other defect, thus restoring the Ir^{4+} ions and Cu^{2+}(A) ions to their pre-illumination concentrations. We use the approximation $E \approx 25kT_m$ to estimate a thermal activation energy for this recovery process.[47-50] Here, T_m corresponds to the temperature where half of the neutral Cu^{3+} acceptors have decayed and half the Ir^{4+} ions have recovered. From Fig. 14, T_m is near 315 °C (or 588 K). This gives a thermal activation energy near E = 1.27 eV.

Since the $Ir^{3+/4+}$ donor level has been experimentally determined to be 2.25 eV below the conduction band minimum,[51] we attribute the decay of the Cu^{3+} ions and recovery of the Ir^{4+} ions in Fig. 14 to the thermal excitation of electrons from the valence band to the neutral Cu acceptors (or equivalently, the release of holes to the valence band). With this interpretation, our analysis of the Cu^{3+} thermal decay places the (0/–) level of the isolated Cu acceptor approximately 1.27 eV

above the valence-band maximum. Recently, Cai *et al.*[4] predicted that the (0/–) level of Cu in β-Ga_2O_3 is 2.02 eV above the valence band maximum. These experimental and calculated values for the Cu (0/–) acceptor level are in reasonable agreement and follow the trend seen for the Mg and Zn (0/–) levels in β-Ga_2O_3 of experimental values being lower than computational values.[1,52]

We now turn to Sample 2, grown by the VGF method, and show the thermal decay and recovery of photoinduced defects in Fig. 15. As was noted earlier, there are significant differences between Samples 1 and 2. In Sample 2, the initial concentration of Cu^{2+}(B) ions is 12 times greater than the concentration of Cu^{2+}(A) ions, whereas the initial concentrations of these two defects are nearly equal in Sample 1. Also, Sample 2 has a higher Fermi level that causes nearly all the iridium donors to initially be in the non-EPR-active neutral Ir^{3+} charge state. In contrast, most of the iridium ions in Sample 1 are initially present as singly ionized Ir^{4+} ions. Infrared absorption gave a value of 1.0×10^{17} cm^{-3} for the "before light" concentration of Ir^{4+} ions in Sample 2, compared to a "before light" value of 4.0×10^{18} cm^{-3} for Ir^{4+} ions in Sample 1.

In Fig. 15, the intensities of the Cu^{2+}(B) and Cu^{3+} EPR spectra are plotted as a function of heating temperature after an exposure to 275 nm light. Production and decay results for the Cu^{3+} optical absorption (measured at 422 nm in Fig. 13) are also included. The Cu^{2+}(A) EPR data have been added in Fig. 15 but are not normalized because the intensities are much reduced compared to Cu^{2+}(B) and do not change significantly with temperature. Figures 14 and 15 can be directly compared since the same steps were followed when taking data. As can be seen, Sample 2 is very different from Sample 1. The Cu^{2+}(B) ions play a central role in Sample 2. Their decrease with light and their thermal recovery directly correlates with the production and decay of the Cu^{3+} ions. This is different from Sample 1 where there was little connection between the Cu^{3+} and Cu^{2+}(B) ions during heating.

The results in Fig. 15 suggest that 275 nm light converts Cu^{2+}(B) ions to Cu^{3+} ions in Sample 2. Since the concentration of Ir^{4+} ions is small in Sample 2, another defect must be serving as the electron trap during the illumination. Both observations can be explained if Cu^{2+}(B) ions play a dual role (i.e., if the probability for a Cu^{2+}(B) ion to trap a hole and become a Cu^{3+} ion is nearly

equal to the probability for a Cu^{2+}(B) to trap an electron and become a Cu^{+} ion). Unfortunately, the mechanisms that lead to this dual behavior have not been clearly identified. One possible scenario that would be consistent with much of the data is based on an OH^{-} ion being the adjacent defect for the Cu^{2+}(B) ions. The 275 nm light could cause the OH^{-} ion to disassociate into an O^{2-} ion and an H^{+}, with the H^{+} moving away from the Cu^{2+} ion and bonding to a more distant oxygen ion.[53,54] After the dissociation of the OH^{-} ion, the Cu^{2+} ion, now with no adjacent defect, could trap a hole and become a Cu^{3+} ion. The remaining Cu^{2+}(B) ions, with the adjacent OH^{-} ion, could trap electrons and become Cu^{+} ($3d^{10}$) ions. These Cu^{+} ions would have no unpaired spins and thus no EPR signal (this would account for the lack of an observable electron trap in Fig. 15). Electrons thermally released from these Cu^{+} ions in the 75-175 °C range would recombine with holes at the Cu^{3+} ions. Another possible scenario begins with an H^{-} ion trapped within an oxygen vacancy as the adjacent defect for the Cu^{2+}(B) ions. This latter model has been explored by Jesenovec *et al*.[5] A final determination of the mechanisms leading to the production and thermal decay of the Cu^{3+} ions in VGF-grown crystals, such as Sample 2, must await further experimental and computational results.

VIII. SUMMARY

Two S = 1/2 EPR spectra, labeled Cu^{2+}(A) and Cu^{2+}(B), are observed in as-grown Cu-doped β-Ga_2O_3 crystals grown by the CZ and VGF methods. The Cu^{2+}(A) ions occupy Ga(2) sites with no nearby defect and have the unpaired spin in a ($3z^2 - r^2$) orbital. The Cu^{2+}(B) ions, also at Ga(2) sites, have the unpaired spin in an ($x^2 - y^2$) orbital because of a defect located at a neighboring oxygen site in the *b*-*c* plane. ENDOR provides further characterization of the Cu^{2+}(A) ions. Exposure at room temperature to 275 nm light produces Cu^{3+} ions and decreases the intensities of the Cu^{2+}(A) and Cu^{2+}(B) spectra. The Cu^{3+} ions have an S = 1 EPR spectrum and are responsible for broad optical absorption bands peaking near 365, 422, 486, 599, and 696 nm. Spin-Hamiltonian parameters are determined for the three EPR spectra.

A series of stepwise thermal anneals after an illumination show that the decay of the Cu^{3+} ions and the recovery of the Cu^{2+}(A) and Cu^{2+}(B) ions happens in the 75 to 375 °C range, with the

CZ-grown and the VGF-grown crystals having quite different responses. The CZ-grown crystal has a simple behavior, as expected for high-quality material containing few unintentional defects. When the 275 nm light is on the CZ crystal at room temperature, singly ionized Ir^{4+} donors convert to neutral Ir^{3+} donors by trapping electrons and singly ionized Cu^{2+}(A) acceptors convert to neutral Cu^{3+} acceptors by trapping holes. Subsequent heating, without light, allows the Cu^{3+} acceptors to release holes to the valence band near 315 °C. An activation energy for this process is estimated to be 1.27 eV. This, in turn, places the (0/–) level for Cu acceptors in β-Ga_2O_3 approximately 1.27 eV above the valence band maximum.

The behavior of the VGF crystal during an illumination and subsequent heating is more complex and reflects the presence of large concentrations of unintentional defects (possibly hydrogen and/or oxygen vacancies). In contrast to the CZ crystal, where the Cu^{3+} ions decay near 315 °C when they release holes, the Cu^{3+} ions in the VGF crystal decay near 125 °C when electrons are released from an unidentified electron trap (most likely Cu^{+} ions). Details of the mechanisms involved in the formation and decay of Cu^{3+} ions in VGF material are not well understood at this time.

ACKNOWLEDGMENTS

T.D.G. was supported at the Air Force Institute of Technology by an NRC Research Associateship Award. Work at WSU was supported by the Air Force Office of Scientific Research under award number FA9550-21-1-0507 monitored by Dr. Ali Sayir. Any opinions, findings, and conclusions or recommendations expressed in this paper are those of the authors and do not necessarily reflect the views of the United States Air Force.

AUTHOR DECLARATIONS

Conflict of Interest

The authors have no conflicts to disclose.

DATA AVAILABILITY

The data that support the findings of this study are available within the article.

REFERENCES

[1]T. D. Gustafson, J. Jesenovec, C. A. Lenyk, N. C. Giles, J. S. McCloy, M. D. McCluskey, and L. E. Halliburton, "Zn acceptors in β-Ga_2O_3 crystals," J. Appl. Phys. **129**, 155701 (2021).

[2]J. Jesenovec, J. Varley, S. E. Karcher, and J. S. McCloy, "Electronic and optical properties of Zn-doped β-Ga_2O_3 Czochralski single crystals," J. Appl. Phys. **129**, 225702 (2021).

[3]D. Skachkov and W. R. L. Lambrecht, "Computational study of electron paramagnetic resonance parameters for Mg and Zn impurities in β-Ga_2O_3," Appl. Phys. Lett. **114**, 202102 (2019).

[4]X. Cai, F. P. Sabino, A. Janotti, and S.-H. Wei, "Approach to achieving a *p*-type transparent conducting oxide: Doping of bismuth-alloyed Ga_2O_3 with a strongly correlated band edge state," Phys. Rev. B **103**, 115205 (2021).

[5]J. Jesenovec, C. Pansegrau, M. D. McCluskey, J. S. McCloy, T. D. Gustafson, L. E. Halliburton, and J. B. Varley, "Persistent photodarkening in Cu-doped β-Ga_2O_3," (submitted to Physical Review Letters, available at https://arxiv.org/abs/2201.01861).

[6]J.-M. Spaeth and H. Overhof, *Point Defects in Semiconductors and Insulators: Determination of Atomic and Electronic Structure from Paramagnetic Hyperfine Interactions* (Springer-Verlag, Berlin, 2003).

[7]J. A. Weil and J. R. Bolton, *Electron Paramagnetic Resonance: Elementary Theory and Practical Applications*, 2nd ed. (John Wiley and Sons, Hoboken, NJ, 2007).

[8]W. E. Blumberg, J. Eisinger, and S. Geschwind, "Cu^{3+} ion in corundum," Phys. Rev. **130**, 900 (1963).

[9]S. A. Marshall, T. T. Kikuchi, and A. R. Reinberg, "Paramagnetic resonance absorption of divalent nickel in α-Al_2O_3 Single Crystal," Phys. Rev. **125**, 453 (1962).

[10]C. Bozdog, K. H. Chow, G. D. Watkins, H. Sunakawa, N. Kuroda, and A. Usui, "Electron paramagnetic resonance of Cu(d^9) in GaN," Phys. Rev. B **62**, 12923 (2000).

[11]M. Saleh, A. Bhattacharyya, J. B. Varley, S. Swain, J. Jesenovec, S. Krishnamoorthy, and K. Lynn, "Electrical and optical properties of Zr doped β-Ga_2O_3 single crystals," Appl. Phys. Express **12**, 085502 (2019).

[12]M. Saleh, J. B. Varley, J. Jesenovec, A. Bhattacharyya, S. Krishnamoorthy, S. Swain, and K. Lynn, "Degenerate doping in β-Ga_2O_3 single crystals through Hf-doping," Semicond. Sci. Technol. **35**, 04LT01 (2020).

[13]J. Jesenovec, C. Remple, J. Huso, B. Dutton, P. Toews, M. D. McCluskey, and J. S. McCloy, "Photodarkening and dopant segregation in Cu-doped β-Ga_2O_3 Czochralski single crystals," J. Cryst. Growth **578**, 126419 (2022).

[14]M. L. Meil'man, "EPR of Fe^{3+} ions in β-Ga_2O_3 crystals," Sov. Phys. Solid State **11**, 1403 (1969).

[15]Z. Galazka, K. Irmscher, R. Schewski, I. M. Hanke, M. Pietsch, S. Ganschow, D. Klimm, A. Dittmar, A. Fiedler, T. Schroeder, and M. Bickermann, "Czochralski-grown bulk β-Ga_2O_3 single crystals doped with mono-, di-, tri-, and tetravalent ions," J. Cryst. Growth **529**, 125297 (2020).

[16]C. A. Lenyk, N. C. Giles, E. M. Scherrer, B. E. Kananen, L. E. Halliburton, K. T. Stevens, G. K. Foundos, J. D. Blevins, D. L. Dorsey, and S. Mou, "Ir^{4+} ions in β-Ga_2O_3 crystals: An unintentional deep donor," J. Appl. Phys. **125**, 045703 (2019).

[17]S. Geller, "Crystal structure of β-Ga_2O_3," J. Chem. Phys. **33**, 676 (1960).

[18]J. Åhman, G. Svensson, and J. Albertsson, "A reinvestigation of β-gallium oxide," Acta Cryst. C **52**, 1336 (1996).

[19]H. Yan, Y. Guo, Q. Song, and Y. Chen, "First-principles study on electronic structure and optical properties of Cu-doped β-Ga_2O_3," Physica B **434**, 181 (2014).

[20]C. Tang, J. Sun, N. Lin, Z. Jia, W. Mu, X. Tao, and X. Zhao, "Electronic structure and optical property of metal-doped Ga_2O_3: a first principles study," RSC Adv. **6**, 78322 (2016).

[21]C. Zhang, F. Liao, X. Liang, H. Gong, Q. Liu, L. Li, X. Qin, X. Huang, and C. Huang, "Electronic transport properties in metal doped beta-Ga_2O_3: A first principles study," Physica B **562**, 124 (2019).

[22]R. D. Shannon, "Revised effective ionic radii and systematic studies of interatomic distances in halides and chalcogenides," Acta Cryst. A **32**, 751 (1976).

[23]N. J. Stone, "Table of nuclear magnetic dipole and electric quadrupole moments," At. Data Nucl. Data Tables **90**, 75 (2005).

[24]T. D. Gustafson, E. M. Golden, E. M. Scherrer, N. C. Giles, A. A. Grabar, S. A. Basun, D. R. Evans, J. E. Slagle, and L. E. Halliburton, "Photoinduced trapping of charge at sulfur vacancies and copper ions in photorefractive $Sn_2P_2S_6$ crystals," J. Appl. Phys. **129**, 085702 (2021).

[25]E. M. Scherrer, N. C. Giles, T. E. R. Dodson, A. A. Grabar, D. R. Evans, S. A. Basun, J. E. Slagle, and L. E. Halliburton, "Charge trapping by iodine ions in photorefractive $Sn_2P_2S_6$ crystals," J. Chem. Phys. **153**, 144503 (2020).

[26]J. E. Stehr, D. M. Hofmann, J. Schörmann, M. Becker, W. M. Chen, and I. A. Buyanova, "Electron paramagnetic resonance signatures of Co^{2+} and Cu^{2+} in β-Ga_2O_3," Appl. Phys. Lett. **115**, 242101 (2019).

[27]J. E. Wertz and J. R. Bolton, *Electron Spin Resonance: Elementary Theory and Practical Applications* (McGraw-Hill Book Company, New York, NY, 1972), Chap. 11.

[28]A. Abragam and B. Bleaney, *Electron Paramagnetic Resonance of Transition Ions* (Oxford University Press, 1970), Chap. 7, pp. 455-466.

[29]Z. Šroubek and K. Ždánský, "Electron spin resonance of Cu^{2+} ion in $CdWO_4$, $ZnWO_4$, and $MgWO_4$ single crystals," J. Chem. Phys. **44**, 3078 (1966).

[30]B. N. Misra and R. Kripal, "Studies of the ground state wave function and the *g*-anisotropy of the Cu^{2+} ion in different lattices," Chem. Phys. **19**, 17 (1977).

[31]A. T. Brant, S. Yang, N. C. Giles, M. Z. Iqbal, A. Manivannan, and L. E. Halliburton, "Oxygen vacancies adjacent to Cu^{2+} ions in TiO_2 (rutile) crystals," J. Appl. Phys. **109**, 073711 (2011).

[32]F. J. Adrian, "Structural implications of nuclear electric quadrupole splittings in high-T_c superconductors," Phys. Rev. B **38**, 2426 (1988).

[33]J. R. Harmer, "Hyperfine spectroscopy – ENDOR," in *EPR Spectroscopy: Fundamentals and Methods*, edited by D. Goldfarb and S. Stoll (John Wiley & Sons, Chichester, 2018), Chap. 16, pp. 331-357.

[34]T. H. Yeom and A. R. Lim, "Study of nuclear quadrupole interactions and quadrupole Raman

processes of ^{69}Ga and ^{71}Ga in a β-Ga_2O_3:Cr^{3+} single crystal," J. Magn. Reson. **200**, 261 (2009).

[35]A. Schnegg, "Very-high-frequency EPR," in *EPR Spectroscopy: Fundamentals and Methods*, edited by D. Goldfarb and S. Stoll (John Wiley & Sons, Chichester, 2018), Chap. 27, pp. 581-602.

[36]J. Telser, "EPR Interactions – Zero-field splittings," in *EPR Spectroscopy: Fundamentals and Methods*, edited by D. Goldfarb and S. Stoll (John Wiley & Sons, Chichester, 2018), Chap. 3, pp. 29-62.

[37]G. D. Watkins, "EPR and ENDOR studies of defects in semiconductors," in *Identification of Defects in Semiconductors*, Vol. 51A, Semiconductors and Semimetals, edited by M. Stavola (Academic Press, 1998), Chap. 1, p. 14.

[38]J. R. Pilbrow, G. R. Sinclair, D. R. Hutton, and G. J. Troup, "Asymmetric lines in field-swept EPR: Cr^{3+} looping transitions in ruby," J. Magn. Reson. (1969) **52**, 386 (1983).

[39]B. J. Gaffney and H. J. Silverstone, "Simulation methods for looping transitions, J. Magn. Reson. **134,** 57 (1998).

[40]J. R. Ritter, J. Huso, P. T. Dickens, J. B. Varley, K. G. Lynn, and M. D. McCluskey, "Compensation and hydrogen passivation of magnesium acceptors in β-Ga_2O_3," Appl. Phys. Lett. **113**, 052101 (2018).

[41]N. Ueda, H. Hosono, R. Waseda, and H. Kawazoe, "Anisotropy of electrical and optical properties in β-Ga_2O_3 single crystals," Appl. Phys. Lett. **71**, 933 (1997).

[42]T. Onuma, S. Saito, K. Sasaki, T. Masui, T. Yamaguchi, T. Honda, and M. Higashiwaki, "Valence band ordering in β-Ga_2O_3 studied by polarized transmittance and reflectance spectroscopy," Jpn. J. Appl. Phys. **54**, 112601 (2015).

[43]K. A. Mengle, G. Shi, D. Bayerl, and E. Kioupakis, "First-principles calculations of the near-edge optical properties of β-Ga_2O_3," **109**, 212104 (2016).

[44]Y.Tanabe and S. Sugano, "On the absorption spectra of complex ions 1.," J. Phys. Soc. Jap. **9**, 753 (1954).

[45]Y.Tanabe and S. Sugano, "On the absorption spectra of complex ions 2.," J. Phys. Soc. Jap. **9**,

766 (1954).

[46]S. Sugano, Y. Tanabe, and H. Kamimura, *Multiplets of Transition-Metal Ions in Crystals* (Academic Press, New York, 1970).

[47]J. T. Randall and M. H. F. Wilkins, "Phosphorescence and electron traps I. The study of trap distributions," Proc. R. Soc. Lond. A **184**, 366 (1945).

[48]A. G. Milnes, *Deep Impurities in Semiconductors* (John Wiley and Sons, New York, 1973), Chap. 9, pp. 227–228.

[49]R. W. Klaffky, B. H. Rose, A. N. Goland, and G. J. Dienes, "Radiation-induced conductivity of Al_2O_3: Experiment and theory," Phys. Rev. B **21**, 3610 (1980).

[50]Y. Jiang, N. C. Giles, and L. E. Halliburton, "Persistent photoinduced changes in charge states of transition-metal donors in hydrothermally grown ZnO crystals," J. Appl. Phys. **101**, 093706 (2007).

[51]J. R. Ritter, K. G. Lynn, and M. D. McCluskey, "Iridium-related complexes in Czochralski-grown β-Ga_2O_3," J. Appl. Phys. **126**, 225705 (2019).

[52]C. A. Lenyk, T. D. Gustafson, S. A. Basun, L. E. Halliburton, and N. C. Giles, "Experimental determination of the (0/–) level for Mg acceptors in β-Ga_2O_3 crystals," Appl. Phys. Lett. **116**, 142101 (2020).

[53]L. Gomes and S. P. Morato, "Resonant OH^- photodissociation in alkali halide crystals," Phys. Rev. B **55**, 8743 (1997).

[54]J. A. Joens, "The dissociation energy of $OH(X^2\Pi_{3/2})$ and the enthalpy of formation of $OH(X^2\Pi_{3/2})$, ClOH, and BrOH from thermochemical cycles," J. Phys. Chem. A **105**, 11041 (2001).

Table I. Spin-Hamiltonian parameters for Cu^{2+}(A) ions in β-Ga_2O_3. Units for the principal hyperfine parameters are MHz. Uncertainties are estimated to be ±0.001 for the *g* values, ±2.0 MHz for the A principal values, and ±1° for the angles.

	Principal values	Principal-axis directions θ (deg)	ϕ (deg)	Directions in crystal
g matrix				
g_1	2.016	86.2	2.0	near *a*
g_2	2.261	90.2	92.0	near *b*
g_3	2.325	3.8	179.1	near *c**
A hyperfine matrix (combined ^{63}Cu and ^{65}Cu)				
A_1	195	76.3	0.0	near *a*
A_2	124	90.0	90.0	near *b*
A_3	176	13.7	179.9	near *c**

Table II. Spin-Hamiltonian parameters for Cu^{2+}(B) ions in β-Ga_2O_3. Units for the principal hyperfine parameters are MHz. Uncertainties are estimated to be ±0.001 for the *g* values, ±2.0 MHz for the A principal values, and ±1° for the angles.

	Principal values	Principal-axis directions θ (deg)	ϕ (deg)	Direction in crystal
g matrix				
g_1	2.053	69.6	340.0	
g_2	2.099	123.3	55.8	
g_3	2.387	40.6	95.7	between *b* and *c**
A hyperfine matrix (combined ^{63}Cu and ^{65}Cu)				
A_1	0	89.2	358.7	
A_2	7	130.1	88.0	
A_3	354	40.1	89.7	between *b* and *c**

Table III. Spin-Hamiltonian parameters from ENDOR for Cu^{2+}(A) ions in β-Ga_2O_3. Units for the principal hyperfine parameters are MHz. Uncertainties are estimated to be ±0.5 MHz for the A principal values, ±0.2 MHz for the P principal values, and ±1° for the angles.

	Principal values	Principal-axis directions θ (deg)	ϕ (deg)	Directions in crystal
A hyperfine matrix for ^{63}Cu				
A_1	198.8	83.3	0.0	near *a*
A_2	106.7	90.0	90.0	near *b*
A_3	172.6	8.7	180.0	near *c**
P nuclear electric quadrupole matrix for ^{63}Cu				
P_1	19.78	89.8	0.0	near *a*
P_2	–6.99	90.0	90.0	near *b*
P_3	–12.79	0.2	180.0	near *c**

Table IV. Spin-Hamiltonian parameters for Cu^{3+} ions in β-Ga_2O_3. Units for the zero-field parameters are GHz. The values for g, D_1, and D_2 were determined by fitting experimental results. D_3 is obtained from D_1 and D_2, using the traceless nature of **D**. Uncertainty in the D values is estimated to be ±0.2 GHz.

	Principal values	Direction of principal axis
g matrix (isotropic)		
g	2.086	
D matrix (zero-field parameters)		
D_1	22.18	near *a*
D_2	3.31	near *b*
D_3	–25.49	near *c**

Figure Captions

FIG. 1. EPR spectra from Cu^{2+}(A) ions in Sample 1 (a Cu-doped β-Ga_2O_3 crystal grown by the Czochralski method). The spectra were taken at 40 K with a microwave frequency of 9.379 GHz. (a) Magnetic field along the *a* direction. The stick diagram above this spectrum identifies the ^{63}Cu and ^{65}Cu hyperfine lines. (b) Magnetic field along the *b* direction. (c) Magnetic field along the *c** direction.

FIG. 2. Angular dependence of the EPR spectrum from Cu^{2+}(A) ions. The direction of the magnetic field is rotated from *a* to *b*, *b* to *c**, and *c** to *a*. Discrete points are from experiment. The solid lines were generated using the parameters in Table I.

FIG. 3. EPR spectra from Cu^{2+}(B) ions in Sample 1, taken at room temperature with a microwave frequency of 9.385 GHz. Stick diagrams above the spectra identify the ^{63}Cu and ^{65}Cu hyperfine lines. Lines marked with asterisks are from Fe^{3+} ions at octahedral Ga(2) sites. (a) Magnetic field along the *a* direction. (b) Magnetic field along the *b* direction. (c) Magnetic field along the *c** direction.

FIG. 4. Angular dependence of the EPR spectrum from Cu^{2+}(B) ions. The direction of the magnetic field is rotated from *a* to *b*, *b* to *c**, and *c** to *a*. Discrete points are from experiment. The solid lines were generated using the parameters in Table II.

FIG. 5. ENDOR spectra from ^{63}Cu and ^{65}Cu nuclei in Cu^{2+}(A) ions. These spectra were taken at 13 K from Sample 1. The microwave frequency was 9.490 GHz and the magnetic field was along the *a* direction. Labels above the lines identify the responsible Cu nucleus. (a) Magnetic field fixed at the second (next-to lowest) EPR line in Fig. 1(a). (b) Magnetic field fixed at the third (next to highest) EPR line in Fig. 1(a).

FIG. 6. Angular dependence of the ^{63}Cu ENDOR lines from the Cu^{2+}(A) ions. The direction of

the magnetic field is rotated from *a* to *b*, *b* to *c**, and *c** to *a*. Discrete points are from experiment. The solid lines were generated using the parameters in Table III.

FIG. 7. EPR spectrum from Cu^{3+} ions in Sample 1 (a CZ-grown β-Ga_2O_3 crystal). The Cu^{3+} ions were produced at room temperature with 275 nm light. This spectrum was taken at room temperature with the magnetic field along the *a* direction and a microwave frequency of 9.377 GHz. The four lines in each set represent ^{63}Cu and ^{65}Cu hyperfine interactions.

FIG. 8. Angular dependence of the Cu^{3+} EPR spectrum. (a) The direction of the magnetic field is rotated in the *a*-*b* plane. (b) The direction of the magnetic field is rotated in the *b*-*c** plane. Experimental results are represented by discrete points. The solid lines were generated using the parameters in Table IV. There are no experimental points above 1.40 T in the lower plot because of the high-field limit of the magnet.

FIG. 9. Energy levels as a function of magnetic field for Cu^{3+} ions (S = 1) in a Cu-doped β-Ga_2O_3 crystal. Observed transitions (i.e., EPR lines) are indicated by red vertical lines. (a) Magnetic field along the *a* direction. (b) Magnetic field 12° from *a* toward *b*.

FIG. 10. Optical absorption spectra from Sample 1, taken at room temperature with unpolarized light propagating along the *a* direction in the crystal. Spectrum 1 was taken before exposure to light. Spectrum 2 was taken after exposure to 275 nm light.

FIG. 11. Polarization effects in the optical absorption from Cu^{3+} ions in Sample 1. Spectrum 1 (with E ∥ *c**) and spectrum 2 (with E ∥ *b*) were taken before exposure to 275 nm. Spectrum 3 (with E ∥ *c**) and spectrum 4 (with E ∥ *b*) were taken after exposure to 275 nm. The inset shows the difference spectrum produced when spectrum 3 (E ∥ *c**) is subtracted from spectrum 4 (E ∥ *b*).

FIG. 12. Thermal decay of the Cu^{3+} optical absorption in Sample 1. Spectra were taken at room temperature with light polarized E ∥ *b* and propagating along the *a* direction in the crystal. Spec-

trum a was taken before exposure to 275 nm light. Spectrum b was taken after exposure to 275 nm light. Spectra c, d, e, and f were taken after heating to 225, 250, 300, and 325 °C, respectively.

FIG. 13. Thermal decay of the Cu^{3+} optical absorption in Sample 2. Spectra were taken at room temperature with light polarized $E \parallel b$ and propagating along the *a* direction in the crystal. Spectrum a was taken before exposure to 275 nm light. Spectrum b was taken after exposure to 275 nm light. Spectra c, d, e, f, and g were taken after heating to 100, 125, 150, 175, and 325 °C, respectively.

FIG. 14. Thermal decay and recovery of EPR and optical absorption spectra in Sample 1 (CZ grown). Intensities of Cu^{2+}(A) EPR (black squares), Cu^{2+}(B) EPR (blue squares), Cu^{3+} EPR (red closed circles), Cu^{3+} optical absorption (red open circles), and Ir^{4+} EPR (green diamonds) are shown.

FIG. 15. Thermal decay and recovery of EPR and optical absorption spectra in Sample 2 (VGF grown). Intensities of Cu^{2+}(A) (black squares), Cu^{2+}(B) EPR (blue squares), Cu^{3+} EPR (red closed circles), and Cu^{3+} optical absorption (red open circles) are shown.

Figure 1

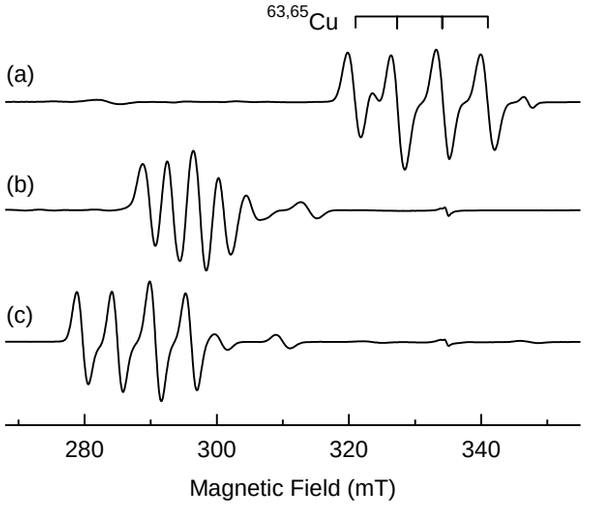

Figure 2

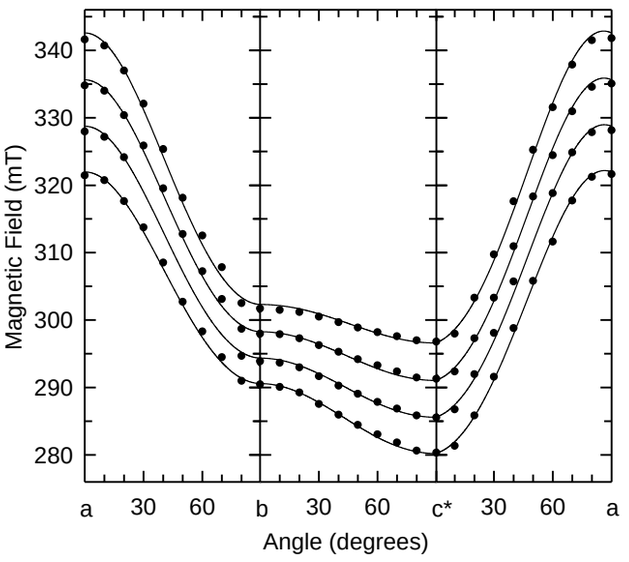

Figure 3

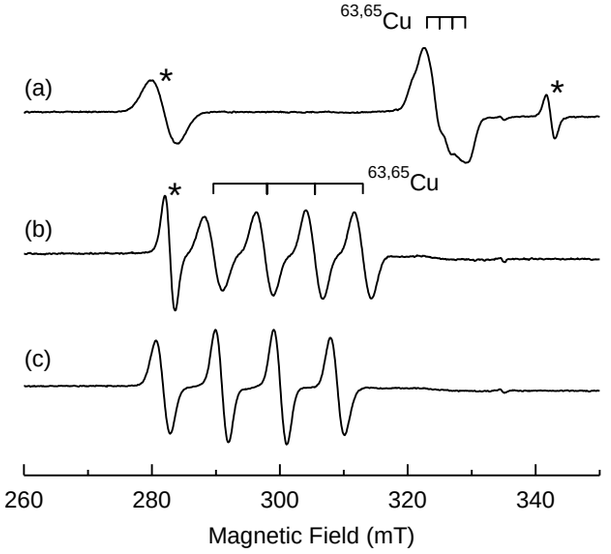

Figure 4

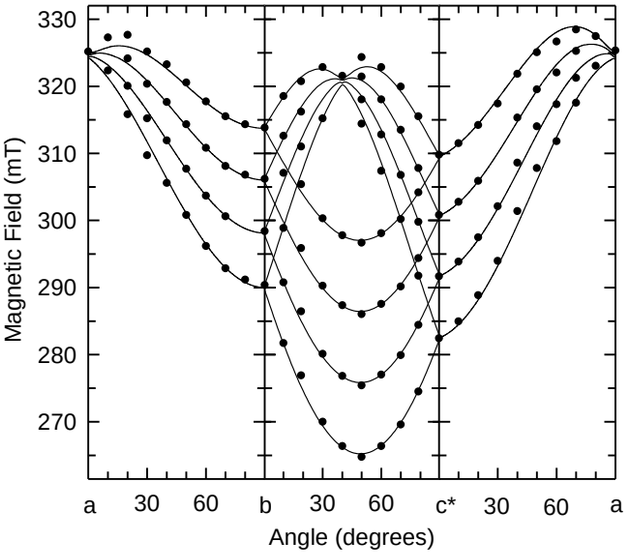

Figure 5

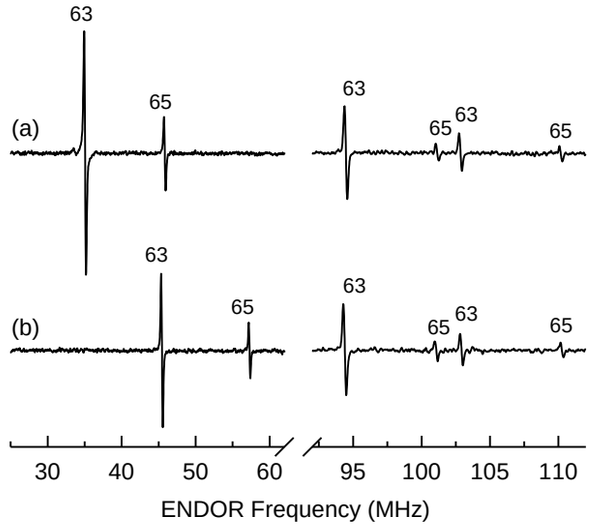

Figure 6

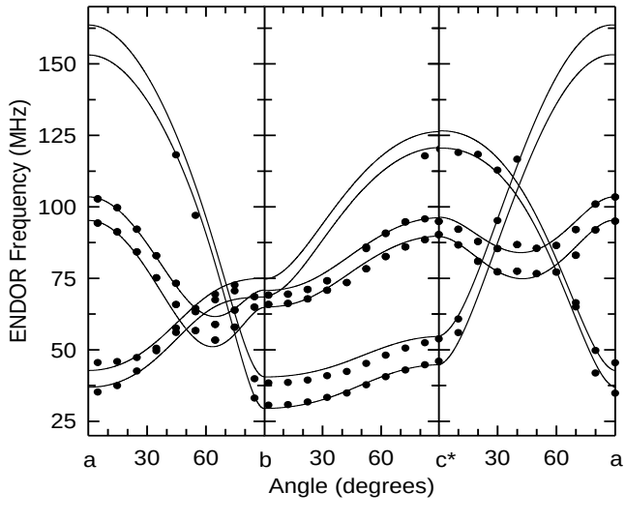

Figure 7

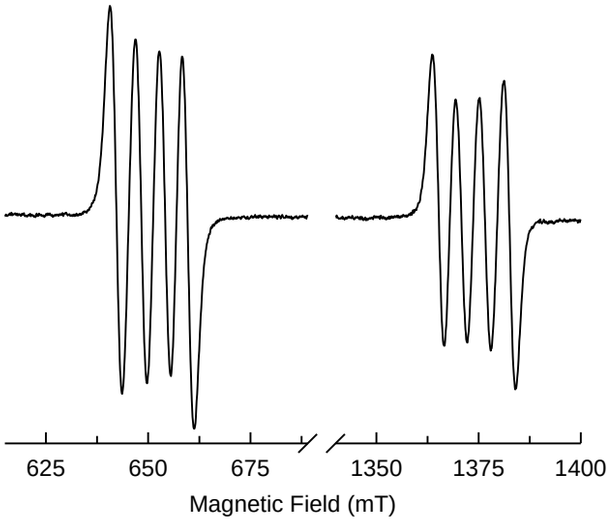

Figure 8

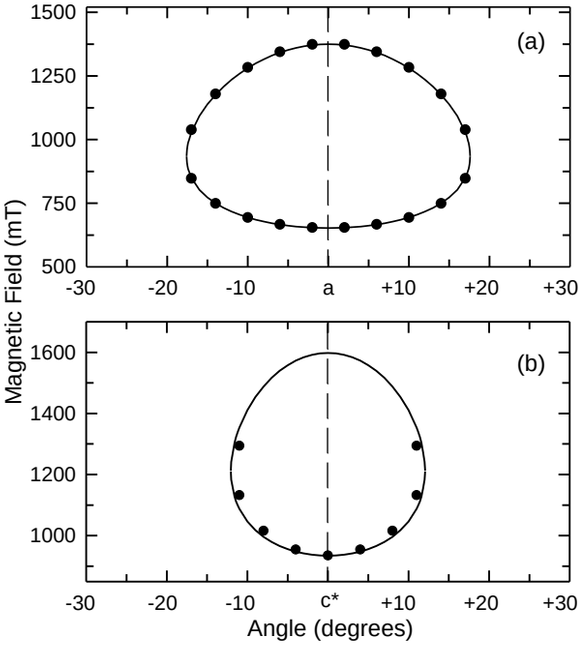

Figure 9

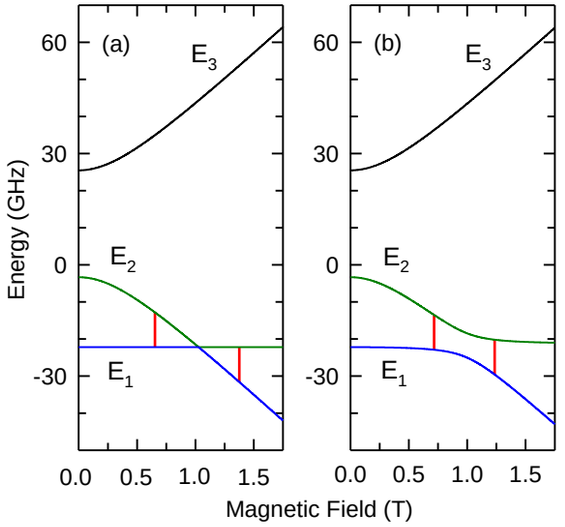

Figure 10

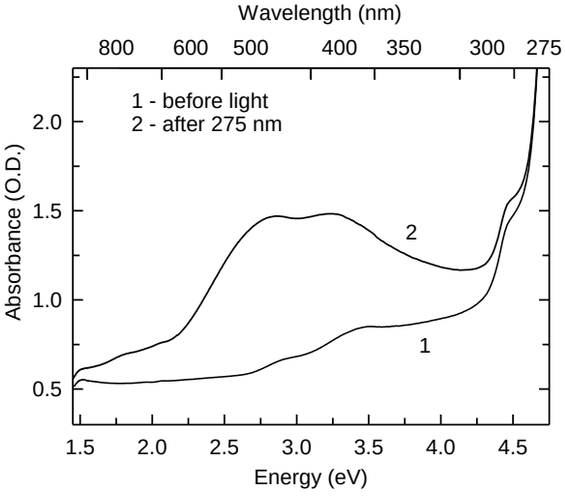

Figure 11

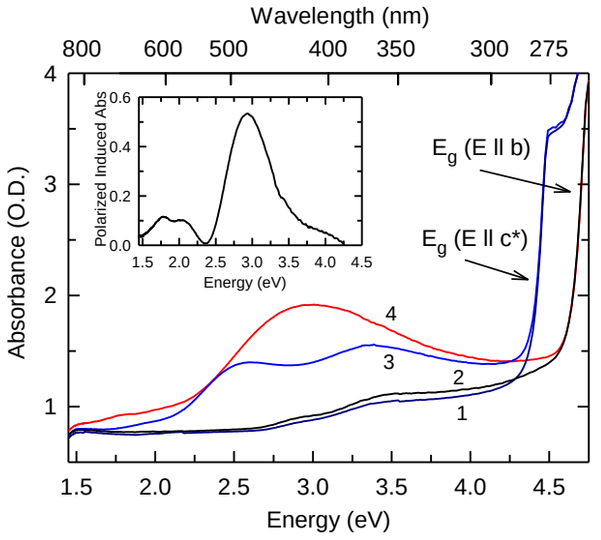

Figure 12

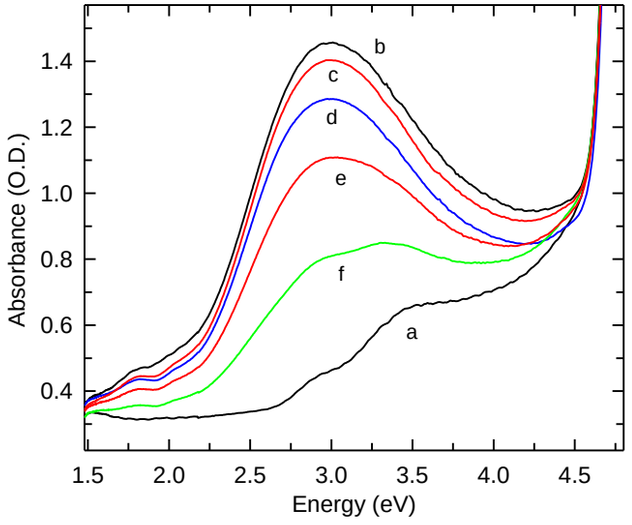

Figure 13

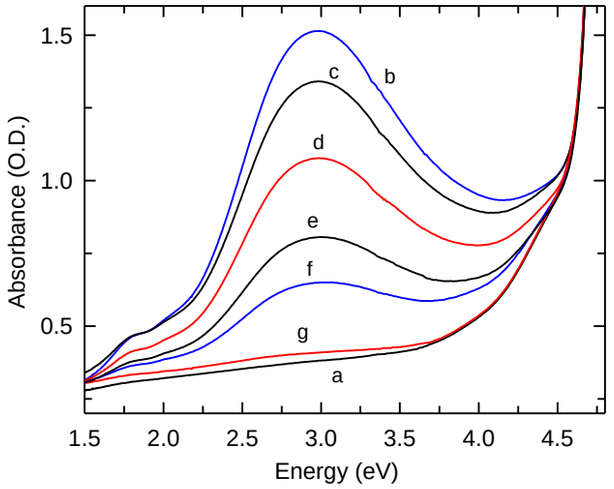

Figure 14

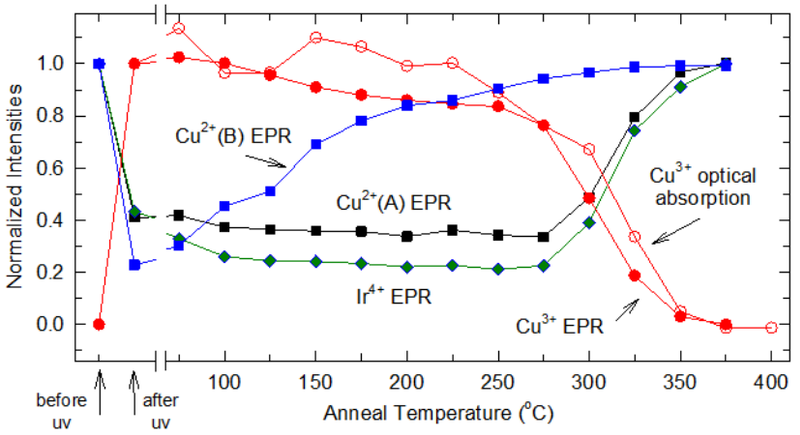

Figure 15

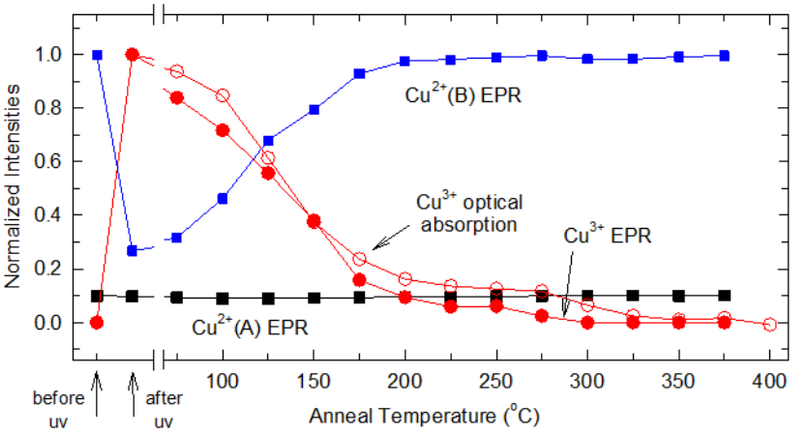

Journal of Applied Physics

PLEASE CITE THIS ARTICLE AS DOI: 10.1063/5.0080502

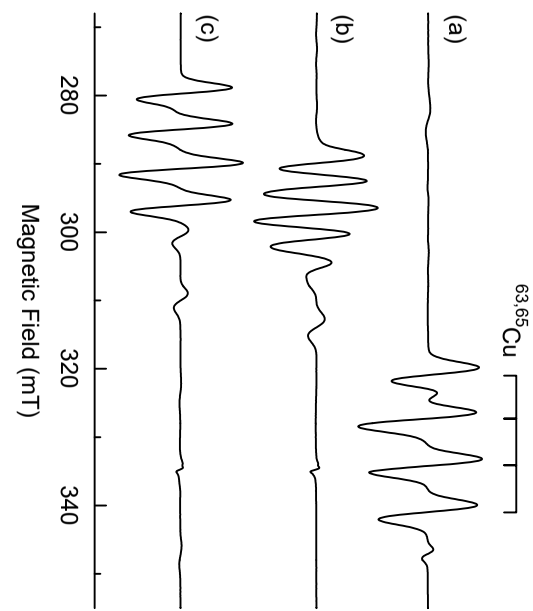

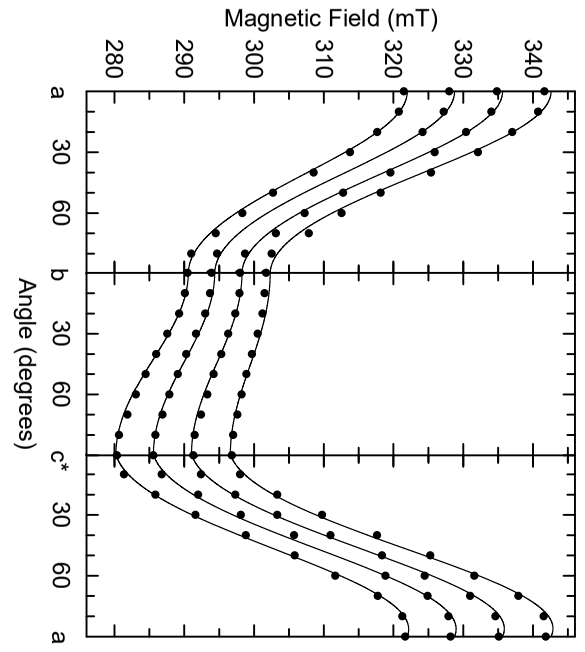

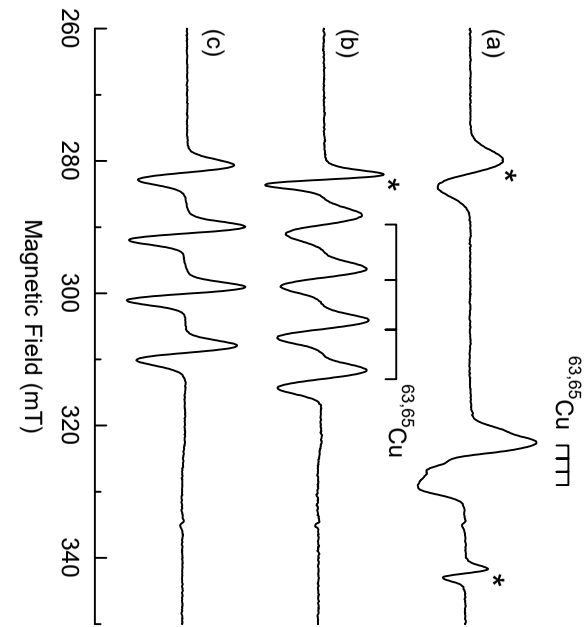

AIP Publishing

Journal of Applied Physics

ACCEPTED MANUSCRIPT

This is the author's peer reviewed, accepted manuscript. However, the online version of record will be different from this version once it has been copyedited and typeset.
PLEASE CITE THIS ARTICLE AS DOI: 10.1063/5.0080502

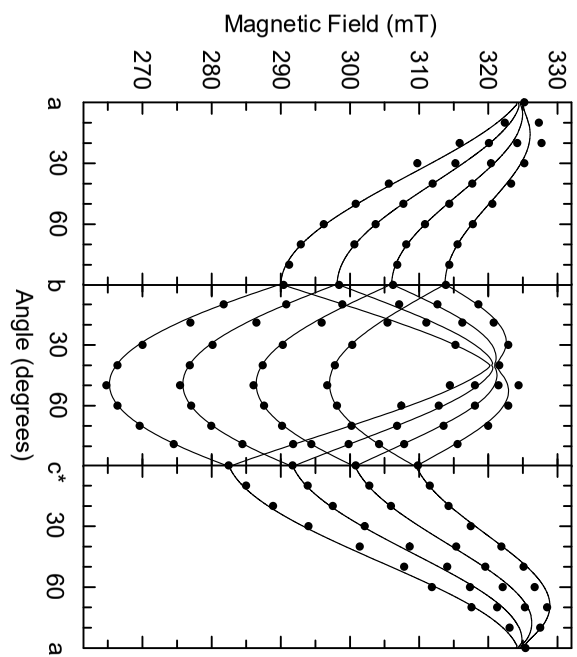

AIP Publishing

Journal of Applied Physics

ACCEPTED MANUSCRIPT

PLEASE CITE THIS ARTICLE AS DOI: 10.1063/5.0080502

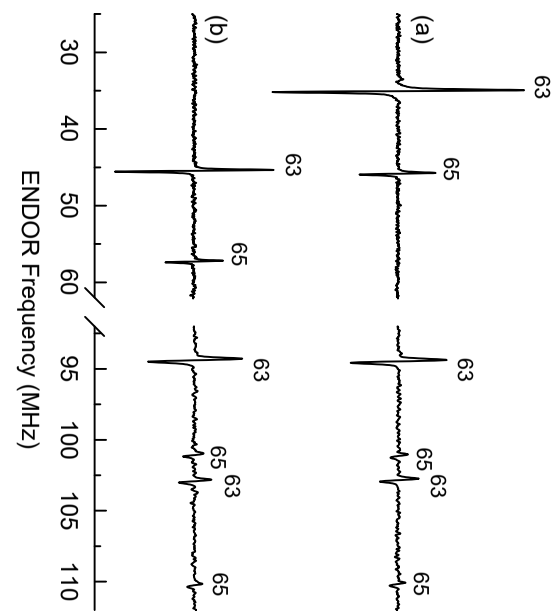

AIP Publishing

Journal of Applied Physics

ACCEPTED MANUSCRIPT

PLEASE CITE THIS ARTICLE AS DOI: 10.1063/5.0080502

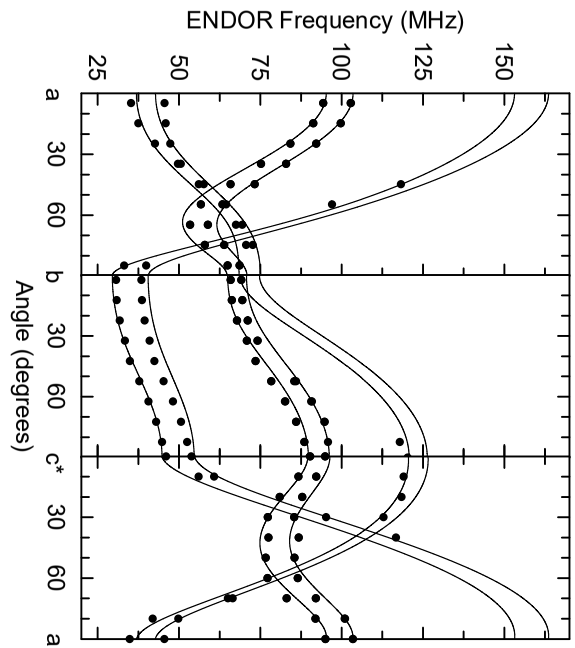

AIP Publishing

Journal of Applied Physics

ACCEPTED MANUSCRIPT

PLEASE CITE THIS ARTICLE AS DOI: 10.1063/5.0080502

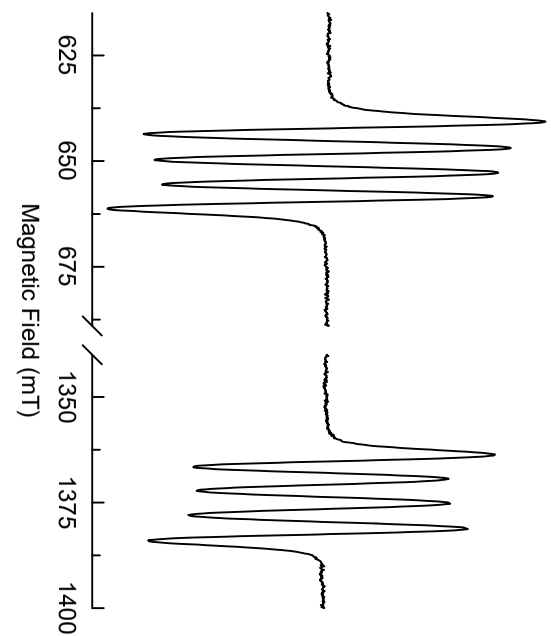

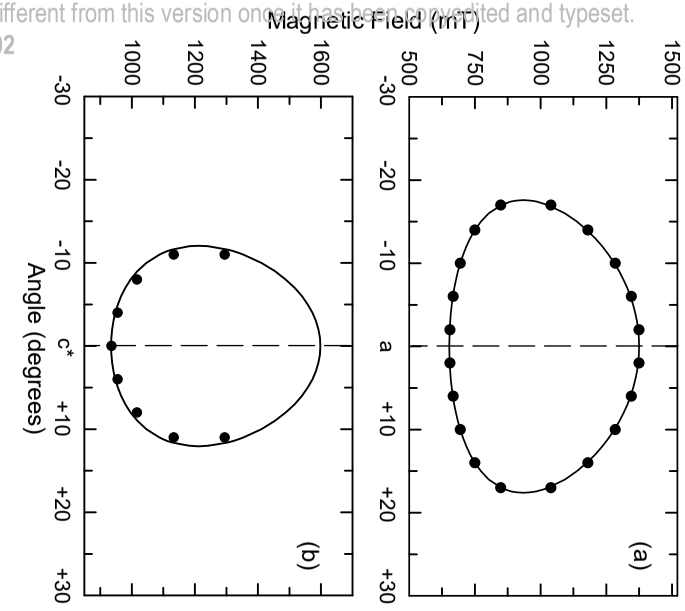

Journal of Applied Physics

PLEASE CITE THIS ARTICLE AS DOI: 10.1063/5.0080502

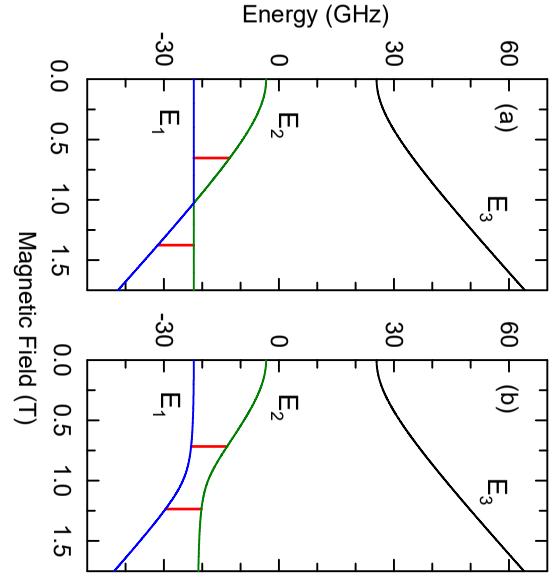

AIP Publishing

Journal of Applied Physics

ACCEPTED MANUSCRIPT

This is the author's peer reviewed, accepted manuscript. However, the online version of record will be different from this version once it has been copyedited and typeset.
PLEASE CITE THIS ARTICLE AS DOI: 10.1063/5.0080502

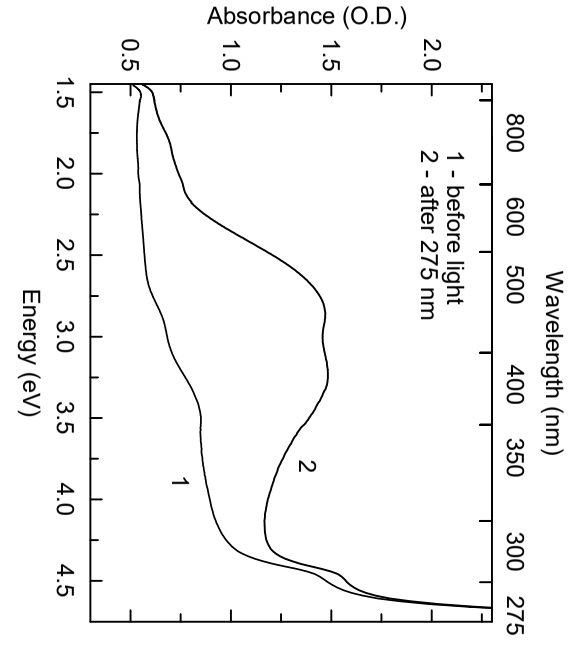

AIP Publishing

Journal of Applied Physics

ACCEPTED MANUSCRIPT

PLEASE CITE THIS ARTICLE AS DOI: 10.1063/5.0080502

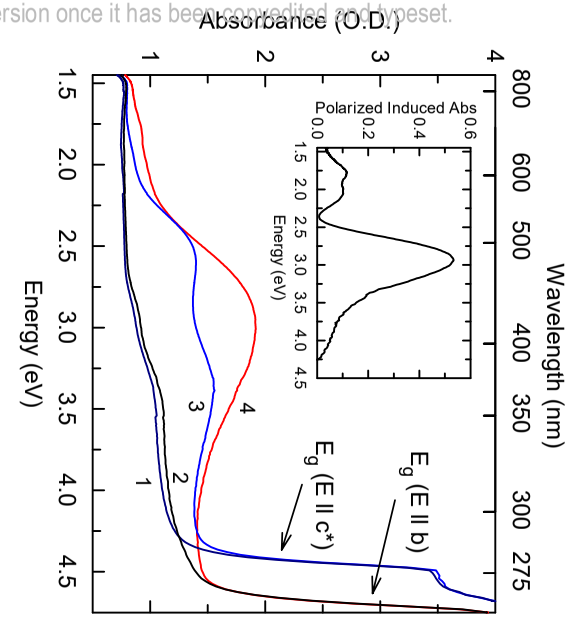

AIP Publishing

Journal of Applied Physics

ACCEPTED MANUSCRIPT

PLEASE CITE THIS ARTICLE AS DOI: 10.1063/5.0080502

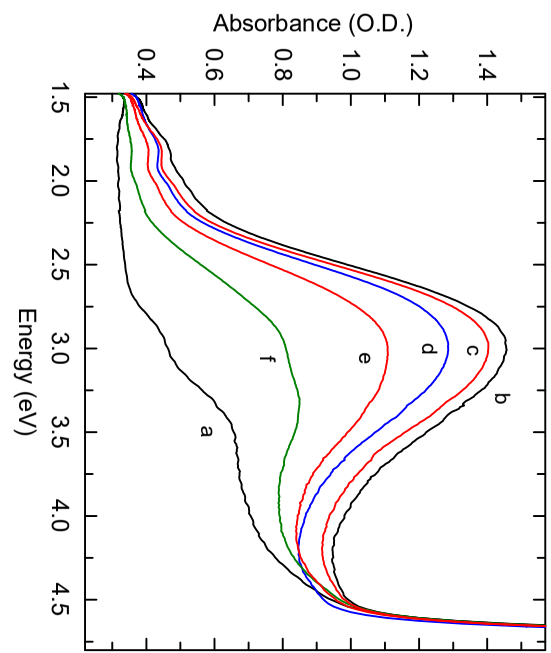

Journal of Applied Physics

PLEASE CITE THIS ARTICLE AS DOI: 10.1063/5.0080502